ISSN 1070-3632, Russian Journal of General Chemistry, 2015, Vol. 85, No. 3, pp. 718–730. © Pleiades Publishing, Ltd., 2015.

Vital Metal Complexes of Levofloxacin as Potential Medical Agents: Synthesis and Their Spectroscopic, Thermal, Computational, and Anticancer Studies[1]

Fatima A.I. Al-Khodir[a,b] and Moamen S. Refat[c,d]

[a] *Department of Chemistry, College of Sciences, Princess Nora Bint Abdul Rahman University, Riyadh, Saudi Arabia*

[b] *Department of Scientific Research, Princess Nora Bint Adul Rahman University, Riyadh, Saudi Arabia*

[c] *Department of Chemistry, Faculty of Sciences, Port Said University, Port Said, Egypt*

[d] *Department of Chemistry, Faculty of Sciences, Taif University, Al-Hawiah, Taif, P.O. Box 888 Zip Code 21974, Saudi Arabia*
e-mail: msrefat@yahoo.com

Received January 25, 2015

Abstract—Metals chelation to biologically active molecules can be used as a medical model of enhancement of their antimicrobial activity. This paper is devoted to synthesis, physicochemical characterization, computational and antimicrobial studies of some complexes of vital metal ions including Ca(II), Fe(III), Pd(II), and Au(III) with levofloxacin (LFX) ligand. Structures of such complexes were elucidated with the help of elemental analyses and spectral measurements (IR, Raman, ^{1}H NMR, ^{13}C NMR and electronic). The accumulated data confirmed that formation of LFX complexes had two coordination pathways as bidentate ligands. One of those proceeded via deprotonation of the carboxylic group followed by bounding to Ca(II) or Fe(III) ion via the carbonyl group and carboxylate oxygen atoms. Alternatively, LFX acted as a neutral ligand bound to Pd(II) or Au(III) ion via nitrogen atoms of the piperazine ring. Molar conductance measurements of the 1 : 1 complexes in DMSO had non-electrolyte nature with the exception of Au(III) complex. Formulae assigned to the complexes were $[Ca(LFX^{-})(Cl)(H_2O)]$ (**I**), $[Fe(LFX^{-})(Cl)_2(H_2O)_2]\cdot 6H_2O$ (**II**), $[Pd(LFX)(Cl)_2)]$ (**III**), and $[Au(LFX)(Cl)_2]\cdot Cl$ (**IV**). The nano-scale nature of Pd(II) and Au(III) complexes has been elucidated on the basis of X-ray powder diffraction (XRD), scanning electron microscope (SEM) and transmission electron microscopy (TEM). The antimicrobial tests of the complexes **I–IV** demonstrated some activity against several kinds of bacteria and fungi. Cytotoxic activity of the complex **IV** was tested against the human colon carcinoma (HCT-116) and human hepatocellular carcinoma (HepG-2) tumor cell lines.

Keywords: metalloantibiotics, levofloxacin, metal ions, complexation, anticancer, nano-scale

DOI: 10.1134/S1070363215030317

INTRODUCTION

The IUPAC name of levofloxacin drug is (*S*)-9-fluoro-2,3-dihydro-3-methyl-10-(4-methylpiperazin-1-yl)-7-oxo-7*H*-pyrido[1,2,3-de]-1,4-benzoxazine-6-carboxylic acid. The levofloxacin drug (LFX, Fig. 1) belongs to the fluoroquinolone family that has a broad spectrum of antibiotic activity against bacteria responsible for respiratory, urinary tract, gastrointestinal, and abdominal infections [1, 2]. LFX has higher activity toward Gram positive than Gram negative bacteria [3, 4]. The metal ions upon complexation with various antibiotic drugs can alter their potential antimicrobial (antibacterial, antitumour, antifungal and antiviral) activity. Metallo-antibiotics interact with proteins, DNA, lipids and RNA helping to recruit new and specific tasks [5–8]. Quinolones act as antibacterial agents by inhibiting both DNA-gyrase (topoisomerase) and DNA topoisomerase enzymes [9, 10]. Quinolones interact with the enzyme-DNA complex forming a drug-enzyme-DNA complex that blocks progression and the replication processes [11, 12]. Zwitterionic nature of quinolones supports their solubility in acidic or basic media [13, 14]. Rarely

[1] The text was submitted by the authors in English.

those act as bidentate ligands coordinated via two carboxyl oxygen atoms or both piperazine nitrogen atoms [13, 14], or monodentate ligands coordinated to the metal ion via the terminal piperazinyl nitrogen atom [15]. Quinolones can bind divalent cations (Mg^{2+}, Ca^{2+}, Cu^{2+}, Zn^{2+}, Fe^{2+}, Co^{2+}) forming chelates with the ratio 1 : 1 or 1 : 2 (metal: ligand) or trivalent cations ($A1^{3+}$, Fe^{3+}) forming chelates with the ratio 1 : 1, 1 : 2, or 1 : 3. The higher stoichiometric ratio (1:4) was detected in complexes of Bi^{3+} [16-18]. The number of coordinated ligands depends on the media pH and type of solvents. In highly acidic media 1 : 1 complexes are favorable whereas 1 : 2 complexes are dominating at higher pH [16]. There were carried out numerous studies regarding complexation between quinolone drugs and metal ions [19–24] and some on coordination between metal ions and fluoroquinolone via nitrogen atoms of the piperazine ring [15, 20, 25].

As the development of our ongoing study of metal-drug interactions [26–30], herein we present synthesis of Ca(II), Fe(III), Pd(II), and Au(III) complexes with LFX drug. To the best of our knowledge LFX complexes with Ca(II) and Fe(III) have not been reported. The only known example of Pd(II) complex with LFX [21] was $[Pd(L)Cl_2]$ in which LFX was coordinated to Pd(II) as a neutral bidentate ligand via the carboxylate and carbonyl oxygen atoms. According to our data, contrary to earlier results [21], Pd(II) ion coordinated in the bidentate fashion via the piperazine nitrogen atoms. Synthesis and characterization of the new Au(III) LFX complex **IV** are important for better understanding the drug-metal ion interaction. Cytotoxic activity of the complex **IV** was tested against the human colon carcinoma (HCT-116) and human hepatocellular carcinoma (HepG-2) tumor cell lines.

EXPERIMENTAL

Chemicals. LFX was received from Aldrich Chemical Co. All chemicals were of analytical grade commercially available from BDH and used without preliminary purification.

Synthesis of $[Ca(LFX^{-})(Cl)(H_2O)]$ (I), $[Fe(LFX^{-})\cdot(Cl)_2(H_2O)_2]\cdot 6H_2O$ (II), $[Pd(LFX)(Cl)_2)]$ (III), and $[Au(LFX)(Cl)_2]\cdot Cl$ (IV). LFX complexes of Ca(II), Fe(III), Pd(II), and Au(III) of 1 : 1 molar ratio were synthesized by refluxing the mixture of the LFX ligand (1 mmol) with the corresponding metal chloride in methanol for 2–3 h at ca 70ºC. For producing complexes **I–IV** ammonia solution (5%) was added dropwise adjusting the media pH to ca 7–8**.** The corresponding coloured precipitate formed immediately and it was filtered off and washed with methanol, diethyl ether and finally dried under vacuum over anhydrous calcium chloride. Yields of products were 80–86%.

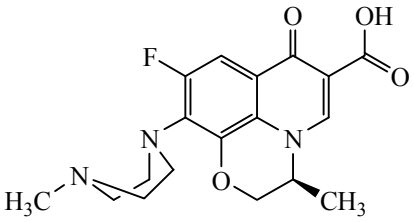

Fig. 1. Structure of levofloxacin antibiotic drug (LFX).

Instruments. CHN analysis was carried out by Vario EL Fab. CHNS. Water and metal content was determined by gravimetric analysis. IR spectra were recorded on Bruker IR spectrophotometer in the range of 400–4000 cm^{-1}. Raman spectra were measured on the Bruker FT-Raman with the laser 50 mW. Molar conductance of 10^{-3} M solutions of the complexes in DMSO was measured on a HACH conductivity meter. All measurements of freshly prepared solutions were taken at room temperature. Electronic spectra (concentration 1×10^{-3} M) were measured in DMSO in the range 200–800 nm by Unicam UV/Vis spectrophotometer. Magnetic susceptibility of LFX complexes was measured using the Gouy's method by a magnetic susceptibility balance from Johnson Metthey and Sherwood. The effective magnetic moment (μ_{eff}) was calculated in accordance with Eqs. (1)–(3) [31].

$$X_g = \frac{C_{Bal}L(R - R_0)}{10^9 M}, \quad (1)$$

where: (R_0) Reading of empty tube; (L) sample length (cm); (M) sample mass (gm); (R) reading for tube with sample; (C_{Bal}) the balance calibration constant = 2.086.

$$X_M = X_g x MW_t. \quad (2)$$

Values of X_M as calculated from Eq. (2) were corrected for diamagnetism of the ligand using Pascal's constants and then applied in the Curie's equation (3).

$$\mu_{eff} = 2.84\sqrt{X_M x T}, \quad (3)$$

where $T = t$ (°C) + 273.

^{1}H and ^{13}C NMR spectra of the products were recorded in DMSO-d_6 solutions on a Bruker 600 MHz spectrometer with TMS as the internal standard. Thermogravimetric analysis (TGA) was conducted using a Shimadzu TGA-50H thermal analyzer. All experiments were performed using a single loose top platinum sample pan under nitrogen atmosphere at the flow rate of 30 mL/min and 10°C/min heating rate within the temperature range 25–800°C. SEM images were obtained using a Jeol Jem-1200 EX II Electron microscope at an acceleration voltage of 25 kV. XRD patterns of the samples were recorded on an X Pert Philips X-ray diffractometer using CuK_{a1} radiation with a graphite monochromator at the scanning rate 0.02°/min. The transmission electron microscopy images were accumulated using a JEOL 100s microscope.

Antimicrobial assessments. Antimicrobial activity of the samples was studied using the modified Kirby-Bauer disc diffusion method [32]. Briefly, the best bacteria/fungi sample (100 μL) was grown in 10 mL of fresh media until it reached the count of ca 108 cells/mL for bacteria or 105 cells/mL for fungi [33]. The microbial suspension (100 μL) was spread onto agar plates. Isolated colonies of each potentially pathogenic organism was collected from the primary agar plates and tested for susceptibility by the disc diffusion method [34, 35]. Of many media available, National Committee for Clinical Laboratory Standards (NCCLS) recommends Mueller-Hinton agar due to its high batch-to-batch reproducibility. In the current study the standard disc diffusion methods developed for filamentous fungi (M38-A) [36] and yeast (M44-P) [37] were applied. The plates were inoculated with filamentous fungi as *Aspergillus Flavus* at 25ºC for 48 h. Gram (+) bacteria as *Staphylococcus Aureus, Bacillus subtilis* and Gram (–) bacteria as *Escherichia Coli*, *Pseudomonas aeruginosa* were incubated at 35–37ºC for 24–48 h. Yeast as *Candida Albicans* were incubated at 30ºC for 24–48 h. Diameters of the corresponding inhabitation zones were measured [32]. Standard discs of Tetracycline (Antibacterial agent), Amphotericin B (Antifungal agent) served as positive controls for antimicrobial activity and filter disc impregnated with 10 μL of a solvent (distilled water and DMSO) were used as a negative control. Composition and pH of the Meuller–Hinton agar were rigorously tested. Blank paper disks (Schleicher & Schuell, Spain) (8.0 mm) were impregnated with 10 μL of a stock solution. Zones of inhibition were measured with slipping calipers in accordance with CLS [34]. The agar-based disk diffusion method was the efficient alternative to the broth methods [38, 39].

Anti-cancer activity. Human colon carcinoma (HCT-116) cells and human hepatocellular carcinoma (HepG-2) cells were obtained from the American type culture collection ATCC, Rockvill, MD. The cells were grown on RPMI-1640 medium supplemented with 10% inactivated fetal calf serum and 50 μg/mL gentamycin. The cells were stored at 37ºC in the humidified atmosphere with 5% CO_2 and subcultured 2–3 times a weak. The cells were grown as monolayers in the growth RPMI-1640 medium supplemented with 10% inactivated fetal calf serum and 50 μg/mL gentamycin. The monolayers of 10000 cells adhered at the bottom of the wells in a 96-well micro titer plate were incubated for 24 h at 37ºC in a humidified incubator with 5% CO_2. The monolayers were washed with sterile phosphate buffered saline (0.01 M pH 7.2) and simultaneously the cells were treated with 100 μL fractions of the diluted test sample in fresh maintenance medium and incubated at 37ºC. Control of untreated cells was made in absence of the test sample. Six wells were used for each concentration of the test sample. The process was monitored under the inverted microscope with the 24 h period. Number of the surviving cells was determined by staining those with crystal violet [40, 41] followed by cell lysing using 33% glacial acetic acid. Reading was taken at 490 nm using ELISA reader (Sun Rise, TECAN, Inc, USA). Percentage of viability was calculated as [1 – (ODt/ODc)] × 100%, where ODt is the mean optical density of wells treated with the test sample and ODc is the mean optical density of untreated cells. The 50% inhibitory concentration (IC_{50}) was estimated from the graphic plots.

RESULTS AND DISCUSSION

Analytical and physical data. Elemental analysis of the LFX complexes **I–IV** indicated their 1 : 1 (metal : ligand) stoichiometry (Table 1). The solid complexes **I–IV** were stable in the air, insoluble in H_2O and most of organic solvents, except DMSO and DMF upon gentle heating. Low molar conductance of the Ca(II), Fe(III), Pd(II) complexes **I–III**, contrary to the Au(III) complex **IV**, revealed the difference in their electrolytic character [42] assigned to absence or presence of chloride ions inside or outside the coordination sphere. The collected data supported the

Table 1. Analytical and physical data for LFX free ligand and metal complexes **I–IV**

Comp. no.	Color	mp, °C	Λ_m, mS	Elemental analysis data, %									
				found					calculated				
				C	H	N	Cl	M	C	H	N	Cl	M
LFX	White	218	4	59.83	5.58	11.63	–	–	–	–	–	–	–
I	White	>250	8	47.45	4.43	9.06	7.71	8.64	47.63	4.66	9.26	7.81	8.83
II	Brown	>250	14	34.01	5.50	6.32	11.06	8.52	34.25	5.59	6.66	11.23	8.85
III	Yellow	>250	18	40.09	3.66	7.54	13.00	19.51	40.13	3.74	7.80	13.16	19.76
IV	Reddish brown	>250	67	32.41	2.98	6.29	15.88	29.44	32.53	3.03	6.32	16.00	29.63

proposed formulae of the synthesized complexes (Fig. 2).

Coordination of LFX towards the metal ions was studied by means of IR, Raman and ^{1}H NMR spectrometry, TGA, and molar conductance. Magnetic moments supported the diamagnetic character of complexes **I–III** and paramagnetic nature of the complex **IV**.

Infrared and Raman spectra. IR data of LFX drug ligand and its complexes **I–IV** are presented in Table 2. The LFX chelating agent had two centers of coordination: either the bidentate coordination via the piperazine nitrogen atoms or carboxylate and carbonyl oxygen atoms depending upon the metal ions [21].

The LFX ligand spectrum contained the broad band at 3419 cm^{-1} which was assigned to stretching vibrations of the OH group (Fig. 3a) involved in H-bonding [43–45]. The carboxylic group of LFX exhibited also the carbonyl group stretching vibration at the higher frequency, 1723 cm^{-1} [44, 45], than the other carbonyl group of the pyridin-4-one.

Complexation of Ca(II), Fe(III), Pd(II), and Au(III) ions with LFX ligand proceeded along two pathways of coordination. Commonly [21] the fluoroquinolones

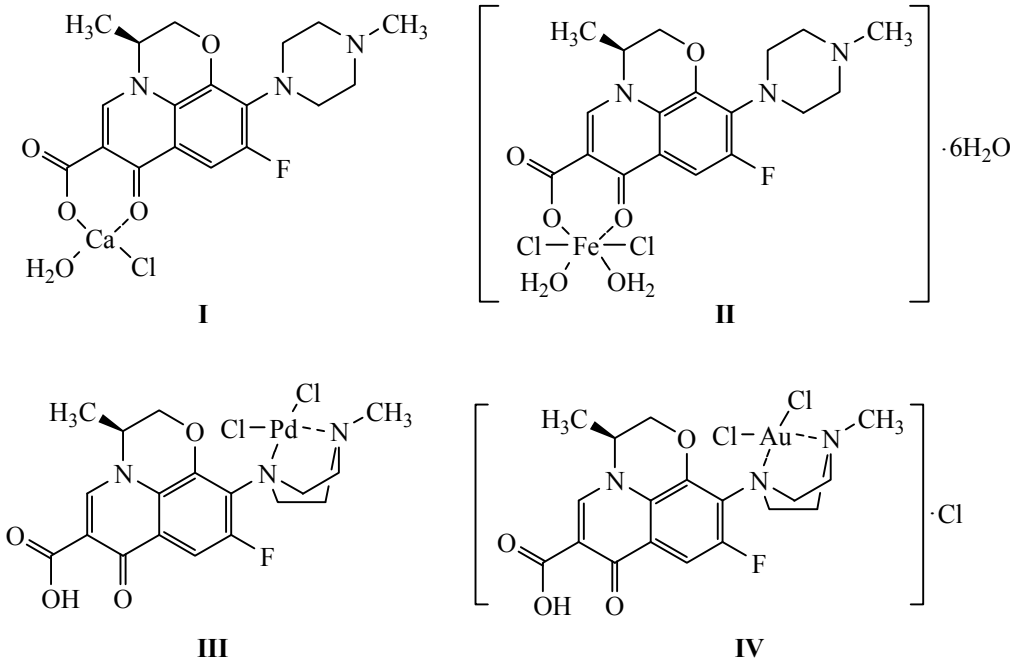

Fig. 2. Suggested formula of $[Ca(LFX^-)(Cl)(H_2O)]$ (**I**), $[Fe(LFX^-)(Cl)_2(H_2O)_2]\cdot 6H_2O$ (**II**), $[Pd(LFX)(Cl)_2)]$ (**III**), and $[Au(LFX)(Cl)_2]\cdot Cl$ (**IV**) complexes.

Table 2. Major IR/Raman spectral bands of LFX free ligand and the complexes **I–IV**

LFX	**I**	**II**	**III**	**IV**	Assignments
3419	3416	3421	3420	3421	ν(OH); COOH + H_2O
3268 3080 3044 2974 2935 2885 2848 2804	3044 2963 2854 2707	3148 3040 2929 2854 2707	3243 3154 2938 2849 2804	3139 3041 2854 2730	ν(CH); CH_2 + CH_3 + $CH_{aromatic}$
1723	–	–	1723	1708	ν(CO); COOH
1620	1583	1521	1620	1624	ν(CO); keto group
–	1622	1622	–	–	ν_{as}(COO)
–	1411	1403	–	–	ν_s(COO)
–	211	219	–	–	$\Delta\nu = [\nu_{as}(COO) - \nu_s(COO)]$
–	575 545	560 509	–	–	ν(M–O)
	–	–	494	492	ν(M–N)
–	375 306	372 331	349 323	361 333	ν(M–Cl); Raman

drugs act as bidentate ligands toward different metal ions via the carboxylate and carbonyl oxygen atoms to form the stable 6-members ring.

According to the first pathway Ca(II) and Fe(III) complexes **I, II** demonstrated no ν(CO) bands of the COOH group at 1723 cm^{-1} typical for LFX ligand [44]. Instead two new bands at ca 1620 and 1400 cm^{-1} assigned to asymmetric and symmetric ν(COO) respectively were registered [44]. The carboxylate group could be attached to metal ions as a monodentate, bidentate or bridging partner. The difference between asymmetric and symmetric frequencies [$\Delta\nu = (\nu_{as}(COO)–\nu_s(COO)]$ could be used as an evidence of the chelation mode of the carboxylate group [44, 45]. For Ca(II) and Fe(III) complexes **I, II** the values Δν were calculated to be 211 and 219 cm^{-1} (Table 2), respectively. Such data supported the monodentate coordination mode of the carboxylate group [46]. The band at 1620 cm^{-1} of the LFX carbonyl group in the complexes **I, II** was shifted to 1583 cm^{-1} and 1521 cm^{-1} respectively indicating the C=O group coordination to the corresponding cation [44]. The bands at ca 3400, 1100 and 600 cm^{-1} were assigned to –OH stretching and angular deformation vibrations of the coordinated and uncoordinated water molecules that were in accord with the elemental analysis and TGM data. The spectra of complexes **I, II** contained bands at (575 and 545) cm^{-1} and (560 and 509) cm^{-1} respectively assigned to the ν(M–O) stretching vibrations [44] indicating LFX ligand coordination toward metal ions as the bidentate ligand.

Second coordination pathway was ligational of the LFX drug with metal ions via the piperazine nitrogen atoms [20]. In the current study, unlike common metal ion complexes of LFX, the drug coordinated to Pd(II) [21] and Au(III) ions in a bidentate manner via the piperazine nitrogen atoms. IR spectra of the complexes **III, IV** demonstrated the ν(C=O) stretching vibration bands of the carboxyl group and new bands at 494 and 492 cm^{-1} assigned to the ν(M-N) stretching vibrations [44, 45] (Table 2).

Electronic spectra and magnetic measurements. The UV-Vis spectrum of LFX demonstrated three characteristic absorption bands at 260, 290 and 330 nm due to π→π* and *n*→π* transitions, respectively [47]. The complex **II** had high spin reflected by two absorption bands at 410 and 320 nm ($^6A_{1g} \rightarrow {}^4T_{2g}$ and $^6A_{1g} \rightarrow {}^4T_{1g}$ transitions) [48, 49]. The band at 280 nm

was assigned to the charge transfer (M→L and L→M charge transfer). The observed magnetic moment of the complex was 5.21 B.M. that corresponded to the octahedral geometry [50, 51]. The electronic spectrum of the complex **IV** demonstrated three essential absorption bands at 500, 365 and 325 nm ($^1A_{1g} \rightarrow {}^1A_{2g}$, $^1A_{1g} \rightarrow {}^1B_{1g}$ and $^1A_{1g} \rightarrow {}^1E_g$, respectively). The band at 280 nm was assigned to charge transfer transition (Table 3). The above bands corresponded to the low-spin square planar configuration [52]. Diamagnetic nature of Au(III) complex **IV** was typical for the low spin d^8 complex with square planar geometry [53].

^1H and ^{13}C NMR spectra. ^{1}H NMR spectrum of the Ca(II) complex **II** was similar to that of LFX but the Au(III) complex **IV** spectrum demonstrated some deviation for hydrogen atoms of the piperazine ring (Table 4).

Thermal analyses. TGA data of the complexes **I**–**IV** (Fig. 3) were in good agreement with the proposed formulae. The curve of the complex (**1**) demonstrated two steps at 260ºC and 550ºC that corresponded to loss of water, $1/2Cl_2$ and LFX (decomposition) fragments (Calculated, %: 87.65. Found, %: 86.97). The final mass of the residue matched well with the formula CaO (Calculated, %: 12.35, Found, %: 13.03). The TG curve of the complex **II** demonstrated four decomposition steps. Two steps (DTG_{max} 212 and 265ºC) were due to loss of six un-coordinated water molecules (Calculated, %: 17.11, Found, %: 16.85). The steps registered at 335 and 560ºC were attributed to complex thermal decomposition that involved loss of two coordinated water molecules, chlorine and LFX (Calculated, %: 70.24. Found, %: 70.00). TG curves of the complexes **III** and **IV** demonstrated the similar pattern with two steps at (340 and 490ºC) and (430 and 520ºC), respectively. The mass loss of Pd(II) complex **III** corresponded to loss of chlorine gas and decomposition of LFX (Calculated, %: 77.27. Found, %: 76.34). The curve of Au(III) complex **IV** demonstrated weight loss of Cl_2, HCl and LFX.

Kinetic thermodynamic study. The kinetic thermodynamic parameters of LFX complexes were computed using the integral method of Coats–Redfern [55] (Table 5). ΔH, ΔS, and ΔG parameters were calculated using the relationships: $\Delta H = E - RT$, $\Delta S = R$ [ln (Ah/kT)] and $\Delta G = \Delta H - T\Delta S$, where k is the Boltzmann's constant and h is the Planck's constant. ΔG increase was attributed to the structural rigidity of the remaining complex upon expulsion of one or more

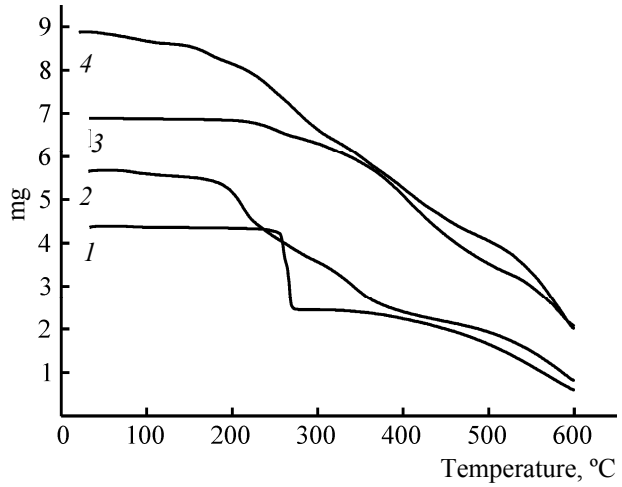

Fig. 3. TG curves of complexes (*1*) [Ca(LFX$^-$)(Cl)(H$_2$O)], (*2*) [Fe(LFX$^-$)(Cl)$_2$(H$_2$O)$_2$]·6H$_2$O, (*3*) [Pd(LFX)(Cl)$_2$)], and (*4*) [Au(LFX)(Cl)$_2$]·Cl.

ligands [56]. Negative values of entropy indicated the higher order of the activated complex compared to that of reactants [57].

XRD, SEM and TEM. Distinctive sharpness of peaks of the products **III** and **IV** in XRD was due to nano-size of the particles. The particles size (D) was calculated from the maximum diffraction patterns using the Debye–Scherrer formula [Eq. (4)] [58].

$$D = \frac{k\lambda}{\beta\cos\theta}, \quad (4)$$

where (λ) the wavelength 1.5418 Å for CuK_α radiation, (k) constant 0.94, (β) full width at half maximum (FWHM) of prominent intensity peak, and (θ) a peak position

The grain sizes were calculated to be 4.00 nm and 3.00 nm for Pd(II) and Au(III) complexes **III** and **IV**, respectively [59]. The strain (ε) was calculated from the slope of β cos θ versus sin θ plot [Eq. (5)].

$$\beta = \frac{\lambda}{D\cos\theta} - \varepsilon\tan\theta. \quad (5)$$

Table 3. Electronic spectra and magnetic moments of complexes [Fe(LFX$^-$)(Cl)$_2$(H$_2$O)$_2$]·6H$_2$O (**II**) and [Au(LFX)(Cl)$_2$]·Cl (**IV**)

Comp. no.	μ_{eff}	Electronic bands/ nm	Geometry
II	5.21 (paramagnetic)	410, 320, 280	Octahedral
IV	0.19 (diamagnetic)	500, 365, 325, 280	Square planar

Table 4. ^{1}H and ^{13}C NMR data of free LFX ligand and the complexes **I** and **IV**

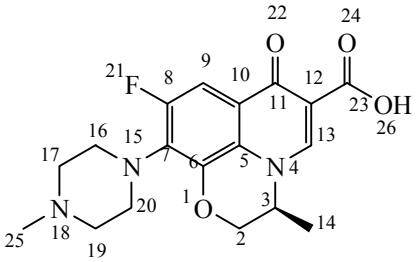

Atom	Chemical shift, δ, ppm					
	LFX [54]		Ca(II)		Au(II)	
	^{1}H NMR spectra	^{13}C NMR spectra	^{1}H NMR spectra	^{13}C NMR spectra	^{1}H NMR spectra	^{13}C NMR spectra
O^{1}	–	–	–	–	–	–
C^{2}	4.94	67.82	4.91	61.75	4.96	–
C^{3}	4.40	–	4.38	-	4.39	–
C^{5}	–	139.78	–	140.50	–	140.23
C^{6}	–	153.58	–	150.30	–	151.20
C^{7}	–	131.84	–	134.42	–	134.47
C^{8}	–	157.06	–	160.85	–	–
C^{9}	7.58	103.20	7.58	106.40	7.63	106.34
C^{10}	–	124.42	–	125.25	–	117.23
C^{11}	–	176.13	–	175.95	–	–
C^{12}	–	106.38	–	106.40	–	106.34
C^{13}	8.96	145.96	8.95	-	8.99	150.27
C^{14}	1.45	17.88	1.44	17.56	1.46	17.51
N^{15}	–	–	–	–	–	–
C^{16}, C^{20}	4.61	50.14	4.59	48.59	4.41	51.97
C^{17}, C^{19}	2.45	54.78	3.34	54.50	3.58	54.48
N^{18}	–	–	–	–	–	–
F^{21}	–	–	–	-	–	–
O^{22}	–	–	–	-	–	–
C^{23}	–	166.00	–	165.80	–	165.82
O^{24}	–	–	–	–	–	–
C^{25}	2.24	46.14	2.26	48.59	2.51	–

Decrease in the strain and dislocation density (δ) [60] indicated formation of high quality complexes (Table 6).

SEM images and TEM scans indicated that the solid products **III** and **IV** were highly monodisperse and the particles size was in the range of 3–4 nm with

Table 5. Kinetic data of LFX complexes based on the Coats–Redfern equation

Complex	Kinetic thermodynamic parameter					r
	E, kJ/mol	A, s^{-1}	ΔS, J mol^{-1} K^{-1}	ΔH, J/mol	ΔG, J/mol	
I	355	4.10×10^{18}	–120	334	240	0.9995
II	75	1.60×10^{5}	–152	72	162	0.9987
III	235	3.00×10^{12}	–150	220	236	0.9990
IV	80	2.10×10^{4}	–164	75	172	0.9997

Table 6. XRD data of complexes [Pd(LFX)$(Cl)_2$)] (**III**) and [Au(LFX)$(Cl)_2$]·Cl (**IV**)

Complexes	2θ	Intensity	d-Spacing	D, nm	$\delta \times 10^{12}$, m^{-2}	$\varepsilon \times 10^{-4}$
III	27.13	1140	3.2842	4	0.0625	0.259
IV	38.20	1146	2.3541	3	0.1111	0.143

the average grain size 3.5 nm (Fig. 4). The complex **IV** nano particles were sticking closely probably due to their aggregation and specific shape [61].

Molecular modeling. The calculated quantum chemical and molecular modeling parameters [62–66] for LFX and the complexes **I–IV** supported their structures [67, 68] (Table 7). The geometry optimization and conformational analysis were performed (Fig. 5, Table 7) by means of semi-empirical PM3 method (Hyperchem 7.5 program) [69]. The quantum chemical parameters were calculated with the help of the following equations [Eqs. (6)–(13)]:

$$\Delta E = (E_{\mathrm{LUMO}}) - (E_{\mathrm{HOMO}}), \quad (6)$$

$$\chi = -\frac{E_{\mathrm{HOMO}} + E_{\mathrm{LUMO}}}{2}, \quad (7)$$

$$\eta = \frac{E_{\mathrm{HOMO}} + E_{\mathrm{LUMO}}}{2}, \quad (8)$$

$$\sigma = \frac{1}{\eta}, \quad (9)$$

$$P_i = -\chi, \quad (10)$$

$$S = \frac{1}{2\eta}, \quad (11)$$

$$\omega = \frac{P_i^2}{2\eta}, \quad (12)$$

$$\Delta N_{\max} = \frac{P_i}{2\eta}. \quad (13)$$

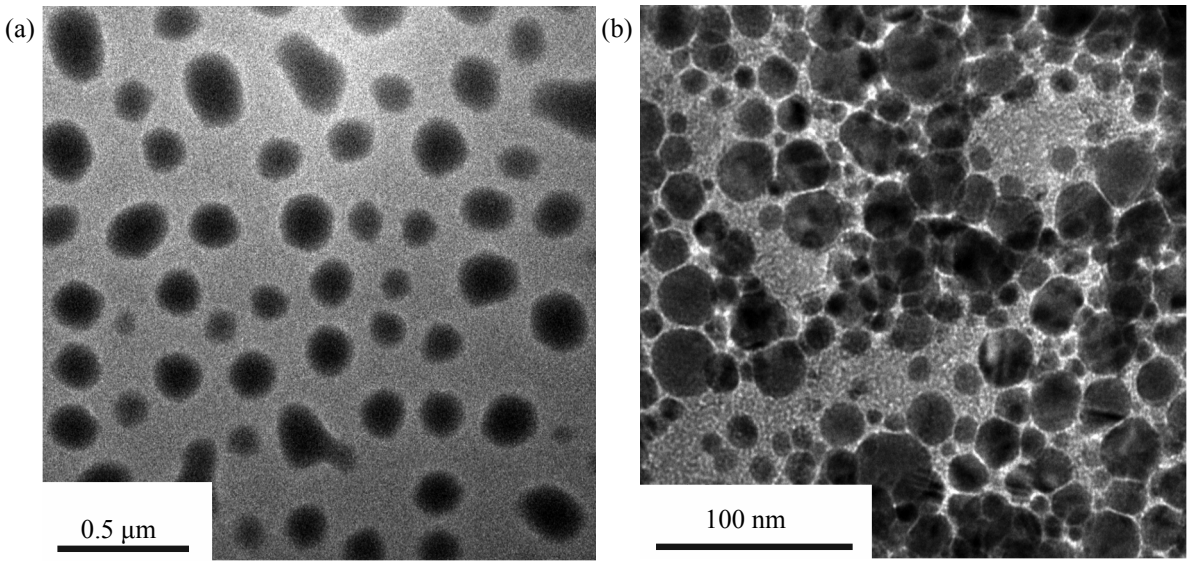

Fig. 4. TEM images of (a) **III** and (b) **IV** NFX complexes.

Table 7. Quantum chemical parameters of LFX ligand and complexes **I–IV**

Parameters	LFX	**I**	**II**	**III**	**IV**
Total energy, a.u.	–151	–176	–196	-198	–163
Binding energy, a.u.	–4.98	–3.74	–5.25	1.197	–7.21
Heat formation, a.u.	0.681	2.32	0.897	7.239	0.109
Electronic energy, a.u.	–974	–133	–1326	–1483	–1271
Dipole moment, Debye	6.71	3.03	14.64	28.68	6.800
E_{HOMO}, eV	–9.990	–9.60	–9.035	–7.019	–7.818
E_{LUMO},eV	–5.751	7.06	7.264	0.623	0.016
ΔE, eV	4.239	16.66	16.30	7.642	7.834
χ , eV	7.87	1.27	0.886	3.198	3.901
η , eV	2.119	8.33	8.15	3.821	3.917
σ, eV	0.472	0.12	1.35	0.262	0.255
P_i, eV	–7.87	–1.27	–0.886	–3.198	–3.901
S, eV	0.236	0.060	0.675	0.131	0.1275
ω, eV	14.62	0.097	0.048	1.338	1.9425
ΔN_{max}, eV	–3.71	–0.153	–0.109	0.837	–0.996

Table 8. Inhibition zone diameters (mm/mg sample) of LFX and the complexes **I–IV** against some kinds of bacteria and fungi

Sample		Inhibition zone diameter, mm/mg					
		B. subtilis (G^+)	*E. coli* (G^-)	*P. aeruginosa* (G^-)	*S. aureus* (G^+)	*A. flavus* (Fungus)	*Candida albicans* (Fungus)
Control: DMSO		0.0	0.0	0.0	0.0	0.0	0.0
Tetracycline Antibacterial agent	Standard	34	32	34	30	–	–
Amphotericin B Antifungal agent	Standard	–	–	–	–	18	19
LFX		36	33	36	29	11	8
I		33	32	30	24	10	12
II		30	34	31	27	12	14
III		37	41	34	31	10	11
IV		45	47	41	35	12	15

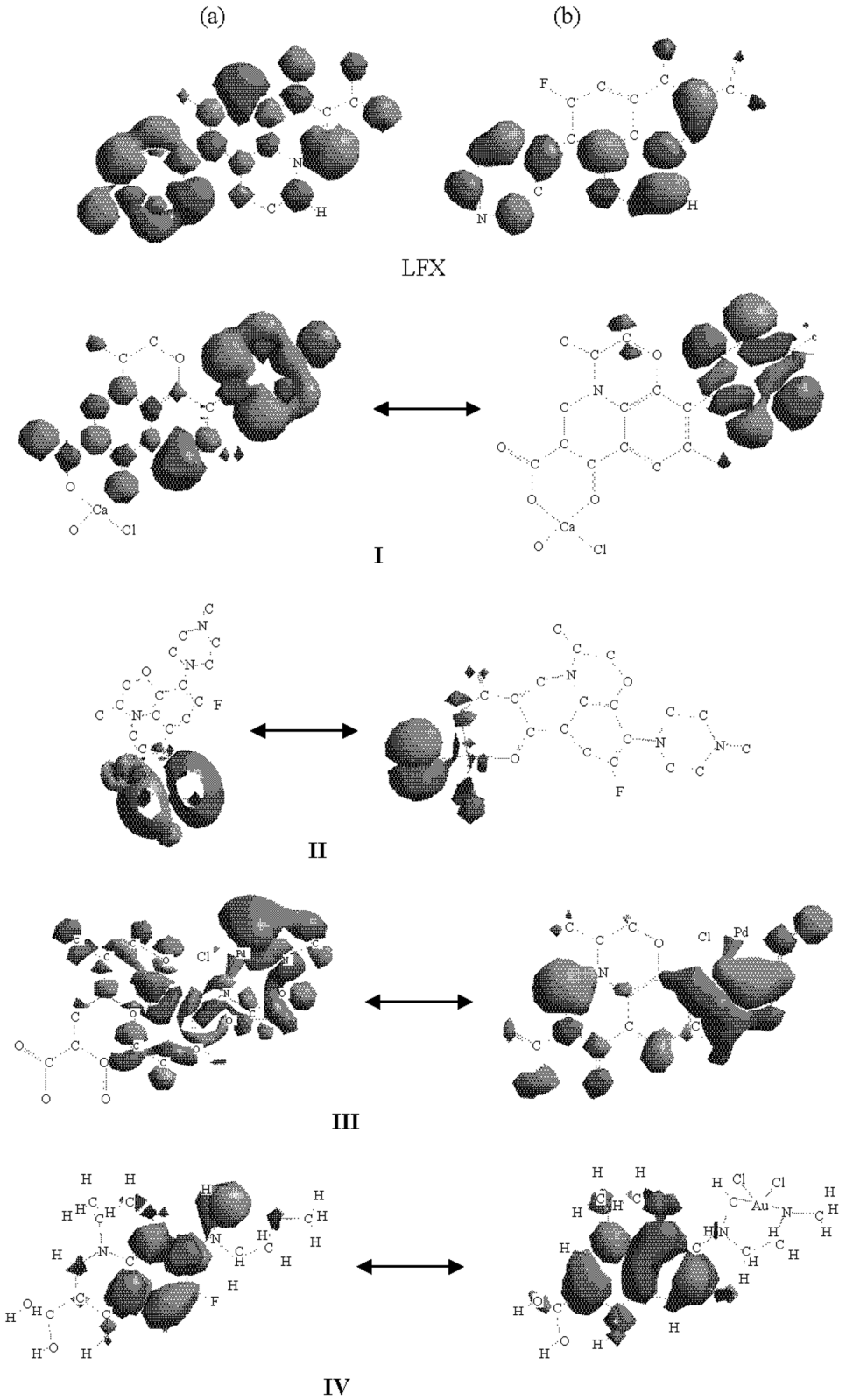

Fig. 5. (a) HOMO and (b) LUMO structures of LFX and its complexes **I–IV.**

Table 9. Inhibitory activities against HCT-116 and HepG-2 cell lines of the complex $[Au(LFX)(Cl)_2]\cdot Cl$ (**IV**) and doxrubcin drug

Concentration, μg	Viability			
	HepG-2 cell line		HCT-116 cell line	
	doxrubcin	Au(III)complex	doxrubcin	Au(III) complex
50.00	4.91	12.46	6.82	9.53
25.00	8.87	34.18	8.89	14.29
12.50	14.83	42.70	14.83	20.42
6.250	16.16	53.89	16.16	39.74
3.125	25.28	76.17	22.28	57.32
1.560	34.64	89.63	34.64	80.41
0.780	45.79	95.38	45.78	88.79
0.390	51.08	99.17	51.28	93.24
0.000	100	100	100	100
IC_{50}	0.467 μg	8.42 μg	0.471 μg	4.43 μg

High values of E_{HOMO} confirmed that LFX ligand had the pronounced donation ability. The calculated global hardness (η) and absolute softness (σ) parameters presented some evidence for the molecular stability and reactivity of the complexes.

Antimicrobial assessments. In vitro antibacterial and antifungal assessments of LFX and its complexes **I–IV** were tested against Gram (+) bacteria as *Staphylococcus Aureus, Bacillus subtilis*; Gram (–) bacteria as *Escherichia Coli*, *Pseudomonas aeruginosa* and Fungi as *Candida Albicans* and *Aspergillus flavus*. Standard discs of tetracycline (antibacterial agent) and amphotericin B as antifungal agents were utilized in this study (Table 8). The antimicrobial activity (antibacterial and antifungal) of LFX and complexes **I–IV** was evaluated by measuring inhibition zones diameter (Table 8). According to the accumulated data the complexes demonstrated higher activity than the free LFX drug. Such effect could be interpreted in terms of overtone's concept of cell permeability and Tweedy's chelation theory [70]. The high antimicrobial activity of the LFX complexes **I–IV** could be assigned to their penetration through the lipid membranes and blocking the metal binding sites in the enzymes of microorganisms. Possibly polarity of the metal ions was reduced by partial sharing of their positive charge with the donor groups and π-electrons delocalization over the whole chelate ring [71].

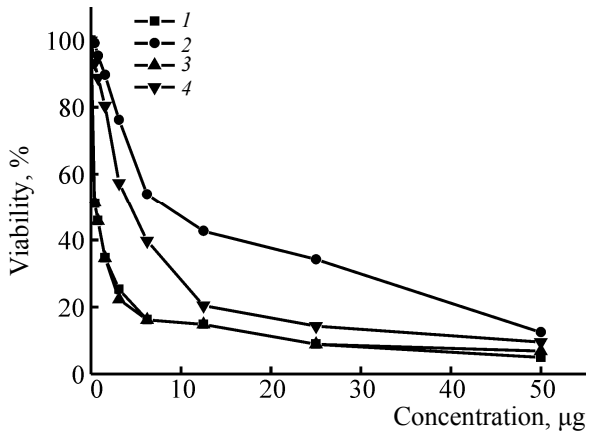

Fig. 6. Curves of inhibitory activity against HCT-116 and HepG-2 cell lines for the Au(III) LFX complex **IV** and doxrubcin drug. (*1*) Doxrubcin HepG-2 cell line, (*2*) Au(III) complex HepG-2 cell line, (*3*) Doxrubcin HCT-116 cell line, and (*4*) Au(III) complex YCT-116 cell line.

In vitro cytotoxicity assessment of the complex **IV** was tested against human colon carcinoma (HCT-116) cell line and human hepatocellular carcinoma (HepG-2) cell line in presence of doxrubcin standard drug (Table 9, Fig. 6). The complex **IV** demonstrated clear potential as an anti-tumor drug.

REFERENCES

1. Nelson, J.M., Chiller, T.M., Powers, J.H., and Angulo, F.J., *Clin. Infect. Dis*., 2007, vol. 44(7), p. 977.
2. Wispelwey, B. and Schafer, K.P., *Expert. Rev. Anti Infect. Ther*., 2010, vol. 8(11), p. 1259.
3. Jones, S.C., Sorbello, A., and Boucher, R.M., *Drug Saf*., 2011, vol. 34(10), p. 839.
4. Stahlmann, R. and Lode, H.M., *Expert. Opin. Drug Saf*., 2013, vol 12(4), p. 497.
5. Ming, L.J., *Med. Res. Rev*., 2003, vol. 23, p. 697.
6. Ogunniran, K.O., Tella, A.C., Alensela, M., and Yakubu, M.T., *African J. Biotechnol*., 2007, vol. 10, p. 1202.
7. Sultana, N. and Arayne, M.S., *Pak. J. Pharm. Sci*., 2007, vol. 20, p. 305.
8. Arayne, S., Sultana, N., Haroon, U., and Mesaik, A.M., *Bioinorg. Chem. Appl.*, 2009, no. 2009,914105.
9. Cozzarelli, N.R., *Science*, 1980, vol. 207, p. 953.
10. Mitscher, L.A., *Chem. Rev*., 2005, vol. 105, p. 559.
11. Hooper, D.C., *Clin. Infect. Dis*., 2000, vol. 31, p. S24.
12. Maxwell, A., *J. Antimicrob. Chemother*., 1992, vol. 30, p. 409.
13. Ross, D. and Riley, C., *Int. J. Pharmaceut*., 1992, vol. 83, p. 267.
14. Takacs-Novak, K., Noszal, B., Hermecz, I., Kereszturi, G., Podanyi, B., and Szasz, G., *J. Pharm. Sci*., 1990, vol. 79, p. 1023.
15. Refat, M.S*., Spectrochim. Acta, Part A*, 2007, vol. 68, p. 1393.
16. Turel, I., Bukovec, N., and Farkas, E., *Polyhedron*, 1996, vol. 15, p. 269.
17. Ma, H., Chiu, F., and Li, R., *Pharm. Res*., 1997, vol. 14, p. 366.
18. El-Roudi, A.M., Soliman, E.M., and Refaiy, S.A., *Afinidad*, 1989, vol. 420, p. 154.
19. Patel, M.N., Gandhi, D.S., and Parmar, P.A., *Inorg. Chem. Commun.*, 2012, vol. 15, p. 248.
20. Gouvea, L.R., Garcia, L.S., Lachter, D.R., Nunes, P.R., de Castro Pereira, F., Silveira-Lacerda, E.P., Louro, S.R.W., Barbeira, P.J.S., and Teixeira, L.R., *Eur. J. Med. Chem.*, 2012, vol. 55, p. 67.
21. Vieira, L.M.M., de Almeida, M.V., Lourenço, M.C.S., Bezerra, F.A.F.M., and Fontes, A.P.S., *Eur. J. Med. Chem*., 2009, vol. 44, p. 4107.
22. Drevenšek, P., Košmrlj, J., Giester, G., Skauge, T., Sletten, E., Sepčić, K., and Turel, I., *J. Inorg. Biochem.*, 2006, vol. 100, p. 1755.
23. Sultana, N., Arayne, M.S., Rizvi, S.B.S., Haroon, U., and Mesaik, M.A., *Med. Chem. Res*., 2013, vol. 22, p. 1371.
24. Tarushi, A., Polatoglou, E., Kljun, J., Turel, I., Psomas, G., and Kessissoglou, D.P., *Dalton Trans*., 2011, vol. 40, p. 9461.
25. Vieira, L.M.M., de Almeida, M.V., de Abreu, H.A., Duarte, H.A., Grazul, R.M., and Fontes, A.P.S., *Inorg. Chim. Acta*, 2009, vol. 362, p. 2060.
26. Refat, M.S. and Mohamed, S.F., *Spectrochim. Acta A*, 2011, vol. 82, p. 108.
27. Refat, M.S., *J. Mol. Str*., 2013, vol. 1037, p. 170.
28. Refat, M.S., *Spectrochim. Acta A*, 2013, vol. 105, p. 326.
29. El-Megharbel, S.M., Hamza, R.Z., and Refat, M.S., *Spectrochim. Acta A*, vol. 131C, p. 534.
30. El-Megharbel, S.M., Hamza, R.Z., and Refat, M.S., *Chemico-Biological Interactions*, 2014, vol. 220, p. 169.
31. Selwood, P.F., *Magnetochemistry*, New York:Wiley Intersci., 1956, 2 ed.
32. Bauer, A.W., Kirby, W.M., Sherris, C., and Turck, M., *Am. J. Clinical Pathology*, 1966, vol. 45, p. 493.
33. Pfaller, M.A., Burmeister, L., Bartlett, M.A., and Rinaldi, M.G., *J. Clin. Microbiol*., 1988, vol. 26, p. 1437.
34. *National Committee for Clinical Laboratory Standards*, *Performance Volume: Antimicrobial Ausceptibility of Flavobacteria*, 1997.
35. *Methods for dilution antimicrobial susceptibility tests for bacteria that grow aerobically. Approved standard M7-A3*, National Committee for Clinical Laboratory Standards, Villanova, Pa, 1993.
36. *Reference Method for Broth Dilution Antifungal Susceptibility Testing of Conidium-Forming Filamentous Fungi*, National Committee for Clinical Laboratory Standards, Proposed Standard M38-A. NCCLS, Wayne, PA, USA, 2002
37. *Methods for Antifungal Disk Diffusion Susceptibility Testing of Yeast*, National Committee for Clinical Laboratory Standards, Proposed Guideline M44-P. NCCLS, Wayne, PA, USA, 2003.
38. Liebowitz, L.D., Ashbee, H.R., Evans, E.G.V., Chong, Y., Mallatova, N., Zaidi, M., and Gibbs, D., *Diagn. Microbiol. Infect. Dis*., 2001, no. 4, p. 27.
39. Matar, M.J., Ostrosky-Zeichner, L., Paetznick, V.L., Rodriguez, J.R., Chen, E., Rex, J.H., *Antimicrob. Agents Chemother*., 2003, vol. 47, p. 1647.
40. Mosmann, T., *J. Immunol. Methods*, 1983, vol. 55, p. 65.
41. Gangadevi, V. and Muthumary, J., *African J. Biotechnology*, 2007, vol. 6, p. 1382.
42. Socrates, G., *Infrared Characteristic Group Frequencies*, New York: John Wiley, 1980.
43. Stuart, B., *Infrared Spectroscopy: Fundamentals and Applications*, New York: John Wiley & Sons, Ltd ISBNs: 0-470-85427-8 (HB); 0-470-85428-6 (PB), 2004.

44. Nakamoto, K., *Infrared Spectra of Inorganic and Coordination Compounds*, New York: Wiley Intersci., 1970, 2 ed.
45. Bellamy, L.J., *The Infrared Spectra of Complex Molecules*, London: Chapman and Hall, 1975.
46. Deacon, G.B. and Phillips, R., *J. Coord. Chem. Rev.*, 1980, vol. 33, p. 227.
47. Sachan, N., Chandra, P., and Yadav, M., *Int. J. Pharm. Pharm. Sci*., 2012, no. 4, p. 383.
48. Ghiladi, R.A., Kretzer, R.M., Guzei, I., Rheingold, A.L., Neuhold, Y., Hatwell, K.R., Zuberbuhler, A.D., and Karlin, K.D., *Inorg. Chem*., 2001, vol. 40, p. 5754.
49. Hamada, Y.Z., Carlson, B.L., and Shank, J.T., *Synth. & React. Inorg. Met. Org. Chem.*, 2003, vol. 33, p. 1425.
50. Cotton, F.A., Goodgame, D.M.L., and Goodgame, M., *J. Am. Chem. Soc*., 1962, vol. 84, p. 167.
51. Figgis, B.N., *Introduction to Ligand Fields*, New York: John Wiley and Sons, 1967, p. 285.
52. Gunasekaran, S. and Uthra, D., *Asian J. Chem.*, 2008, vol. 20(8), p. 6310.
53. Abdalrazaq, E.A., Buttrus, N.H., and Abd Al-Rahman, A.A., *Asian J. Chem.*, 2010, vol. 22(3), p. 2179.
54. Galani, A., Efthimiadou, E.K., Theodosiou, T., Kordas, G., and Karaliota, A., *Inorg. Chim. Acta*, 2014, vol. 423, p. 52.
55. Coats, A.W. and Redfern, J.P., *Nature*, 1964, vol. 201, p. 68.
56. Yusuff, K.K.M. and Sreekala, R., *Thermochim. Acta,* 1990, vol. 159, p. 357.
57. Frost, A.A. and Peasron, R.G., *Kinetics and Mechanism*, New York: Wiley, 1961.
58. Cullity, B.D., *Elements of X-ray Diffraction*, Addison-Wesley, Reading, MA, 1972, p. 102.
59. Salavati-Niasari, M., Mohandes, F., Davar, F., Mazaheri, M., Monemzadeh, M., and Yavarinia, N., *Inorg. Chim. Acta*, 2009, vol. 362(10), p. 3691.
60. Velumani, S., Mathew, X., and Sebastian, P.J., *Solar Energy Mater. Solar Cells*, 2003, vol. 76, p. 359.
61. Carotenuto, G. and Nicolais, F., *Materials*, 2009, no. 2, p. 1323.
62. Pearson, R.G., *J. Org. Chem*., 1989, vol. 54, p. 1423.
63. Geerlings, P., De Proft, F., and Langenaeker, W., *Chem. Rev*., 2003, vol. 103, p. 1793.
64. Parr, R.G., *J. Am. Chem. Soc*., 1999, vol. 121, p. 1922.
65. Chattaraj, P.K. and Giri, S., *J. Phys. Chem. A*, 2007, vol. 111, p. 11116.
66. Speie, G., Csihony, J., Whalen, A.M., and Pie-Pont, C.G., *Inorg. Chem*., 1996, vol. 35, p. 3519.
67. Yousef, T.A., Abu El-Reash, G.M., and El Morshedy, R.M., *J. Mol. Struct*., 2013, vol. 1045, p. 145.
68. Helal, M.H., El-Awdan, S.A., Salem, M.A., Abd-elaziz, T.A., Moahamed, Y.A., El-Sherif, A.A., and Mohamed, G.A.M., *Spectrochim. Acta A*, 2015, vol. 135, p. 764.
69. *HyperChem. Version 7.51*, Hyper Cube, INC.
70. Raman, N., Kulandaisamy, A., and Chinnathangavel Thangaraja, *Trans. Metal Chem*., 2004, vol. 29, p. 129.
71. Tabassum, S., Asim, A., Arjmand, F., Arjmand, F., Mohd Afzal, and Bagchi, V., *Eur. J. Med. Chem*., 2012, vol. 58, p. 308.